

X-Ray Studies of HESS J1809–193 with Suzaku

Takayasu ANADA¹, Aya BAMBA^{2,1,*}, Ken EBISAWA¹, and Tadayasu DOTANI¹

¹*Institute of Space and Astronautical Science, JAXA, 3-1-1 Yoshinodai, Sagamihara, Kanagawa 229-8510*

²*School of Cosmic Physics, Dublin Institute for Advanced Studies 31 Fitzwilliam Place, Dublin 2, Ireland*

(Received ; accepted)

Abstract

Suzaku observed the region including HESS J1809–193, one of the TeV unidentified (unID) sources, and confirmed existence of the extended hard X-ray emission previously reported by ASCA, as well as hard X-ray emission from the pulsar PSR J1809–1917 in the region. One-dimensional profile of the diffuse emission is represented with a Gaussian model with the best-fit σ of 7 ± 1 arcmin. The diffuse emission extends for at least 21 pc (at the 3σ level, assuming the distance of 3.5 kpc), and has a hard spectrum with the photon index of $\Gamma \sim 1.7$. The hard spectrum suggests the pulsar wind nebula (PWN) origin, which is also strengthened by the hard X-ray emission from PSR J1809–1917 itself. Thanks to the low background of Suzaku XIS, we were able to investigate spatial variation of the energy spectrum, but no systematic spectral change in the extended emission is found. These results imply that the X-ray emitting pulsar wind electrons can travel up to 21 pc from the pulsar without noticeable energy loss via synchrotron emission.

Key words: gamma rays: observations — ISM: individual (HESS J1809–193) — stars: pulsars: individual (PSR J1809–1917) — X-rays: ISM

1. Introduction

Galactic plane survey with the H.E.S.S. Cherenkov telescope system revealed dozens of the new very-high-energy (VHE) γ -ray sources (Aharonian et al. 2005a; Aharonian et al. 2006a). Many of them have no counterparts in other wave-lengths, thus called “unidentified (unID) TeV sources”. Today, about 40 such unidentified TeV sources are known on the Galactic plane (Hinton 2007). Most of them are located within a height of ± 1 degree from the Galactic plane, and some are intrinsically extended. Despite a large number of intensive studies in the last several years, their origin is unclear (Hinton 2007).

X-ray follow-up observations of the unID TeV sources are now on-going. Although supernova remnants (SNRs) or hypernova remnants were suggested to be major counterpart

* Corresponding author: abamba@cp.dias.ie

candidates of these TeV unID sources (Yamazaki et al. 2006; Ioka & Meszaros 2009), only a few sources have been actually identified as SNRs (Nakamura et al. 2009; Aharonian et al. 2008). On the other hand, rather surprisingly, several unID TeV sources have been identified as pulsar wind nebulae (PWNe) (Anada et al. 2009; Uchiyama et al. 2009, for example). They seem to be rather old, previously unknown PWNe, compared to the PWNe already identified and well studied in X-rays.

The first HESS observations of the region around PSR J1809–1917 were made from May through June 2004 as part of the systematic survey of the inner Galaxy (Aharonian et al. 2005a; Aharonian et al. 2006a). Because marginal VHE γ -ray signals were detected, HESS J1809–193 was observed again in 2004 and 2005, and significant γ -ray emission was confirmed (Aharonian et al. 2007). Recent study of this source by HESS was reported by Renaud et al. (2008). Fitting the excess map with a 2-D symmetric Gaussian, the best fit position and intrinsic source extension (in rms) were determined as (RA, Dec) = ($18^{\text{h}}09^{\text{m}}52^{\text{s}}$, $-19^{\circ}23'42''$) and $0^{\circ}.25 \pm 0^{\circ}.02$, respectively.

PSR J1809–1917 is a radio pulsar discovered by the Parkes Multibeam Pulsar Survey (Morris et al. 2002). The pulsar is located at the position of (RA, Dec) = ($18^{\text{h}}09^{\text{m}}43^{\text{s}}.1$, $-19^{\circ}17'38''$) with a pulse period of $P = 82.7$ ms and the period derivative of $\dot{P} = 2.55 \times 10^{-14}$ s s $^{-1}$. The distance to the source was estimated to be $d = 3.5$ kpc from the pulsar’s dispersion measure using the NE2001 Galactic electron-density model (Cordes & Lazio 2002). The characteristic age and the spin-down luminosity are $\tau_c = 51$ kyr and $\dot{E} = 1.8 \times 10^{36}$ ergs s $^{-1}$, respectively.

The γ -ray spectral analysis performed by Komin et al. (2007) indicated that the spectral slope is different between the regions near the pulsar and far from the pulsar. This is the second case that spatial variation of the spectral slope is revealed in the VHE γ -ray emission. The first case is HESS J1825–137 (Aharonian et al. 2006b), which is largely extended in both VHE γ -ray and X-ray bands (Uchiyama et al. 2009).

ASCA observation revealed diffuse, non-thermal emission in the vicinity of PSR J1809–1917 (Bamba et al. 2003a). Kargaltsev & Pavlov (2007) detected a bright point X-ray source which was positionally consistent with the pulsar PSR J1809–1917, and resolved the surrounding compact PWN utilizing the very high angular resolution of Chandra. The PWN has a “head-tail” profile, consisting of the southern-head, which is coincident to the pulsar, and the northern-tail. Kargaltsev & Pavlov (2007) claimed that this cometary morphology is attributed to a bow shock created by the pulsar moving supersonically to the southern direction. However, it is still unknown whether the faint diffuse emission discovered by ASCA is related to the PWN or not. In this paper, we make detailed analysis of the diffuse emission for the first time using Suzaku. Suzaku, characterized by the low detector background compared to Chandra and XMM-Newton, is very suitable for the analysis of faint and diffuse X-ray emission such as HESS 1809–193.

2. Observations

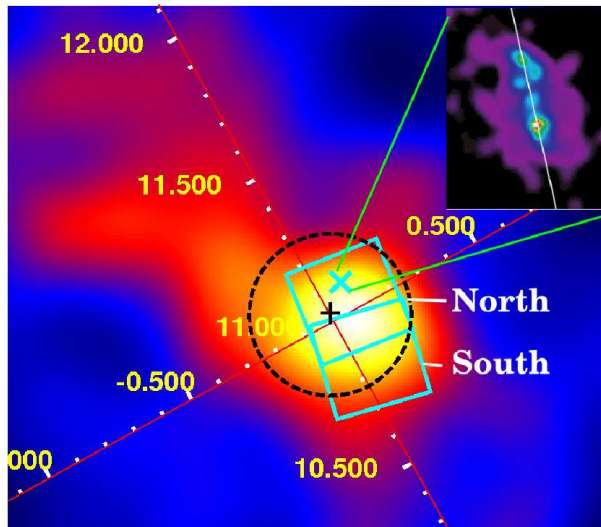


Fig. 1. A smoothed excess map measured by HESS around HESS J1809–193 (Aharonian et al. 2007). Position of the pulsar PSR J1809–1917 is marked with a cyan cross, whose Chandra image (Kargaltsev & Pavlov 2007) is shown in the inset at the top right of the figure. The best fit position and extent of the γ -ray source is marked with a black cross and a dashed circle, respectively. Two cyan squares indicate the two XIS field of views (FOVs) during the Suzaku observations, which are referred to as the North and the South pointing, respectively.

We observed HESS J1809–193 with Suzaku (Mitsuda et al. 2007) in April, 2008. Suzaku is equipped with two types of instruments: the X-ray Imaging Spectrometers (XIS: Koyama et al. 2007) at the foci of four X-Ray Telescopes (XRT: Serlemitsos et al. 2007) and the Hard X-ray Detector (HXD: Takahashi et al. 2007, Kokubun et al. 2007). The observation was carried out with two pointings at north and south of the source region (figure 1) in order to cover the pulsar and extended VHE γ -ray emission along the direction of the elongated shape of the PWN (Kargaltsev & Pavlov 2007). Three XISs (XIS 0, 1, 3) out of four were operated in the normal clocking mode with the Spaced-row Charge Injection (SCI) (Nakajima et al. 2008). We analyzed the data processed by the version 2.2 pipeline. We are interested in the spatial variations of a scale of arcminutes. Hence, we concentrated on the analysis of the XIS data in this paper, since the HXD does not have a spatial resolution within a field of view of ~ 30 arcmin. (FWHM). We applied the standard screening criteria to the XIS data¹ to obtain the cleaned event lists. After the data screening, the net exposures was 51.5 ks and 44.2 ks for the north and south pointing of XIS, respectively. The Suzaku observation log and exposure are summarized in table 1. We used HEADAS version 6.5 software package for the data analysis.

¹ http://www.astro.isas.jaxa.jp/suzaku/process/v2changes/criteria_xis.html

Table 1. Journal of the Suzaku observations of HESS J1809–193

	North	South
Sequence ID	503078010	503079010
Start time (UT) ¹	2008/03/31 14:06	2008/04/01 16:34
End time (UT) ¹	2008/04/01 16:30	2008/04/02 14:47
Aim point R.A. (J2000.0)	18 ^h 09 ^m 37 ^s .4	18 ^h 09 ^m 21 ^s .0
Aim point Decl. (J2000.0)	−19°21′24″	−19°32′02″
Net exposure (ks)	51.5	44.2

¹ Time form of yyyy/mm/dd hh:mm

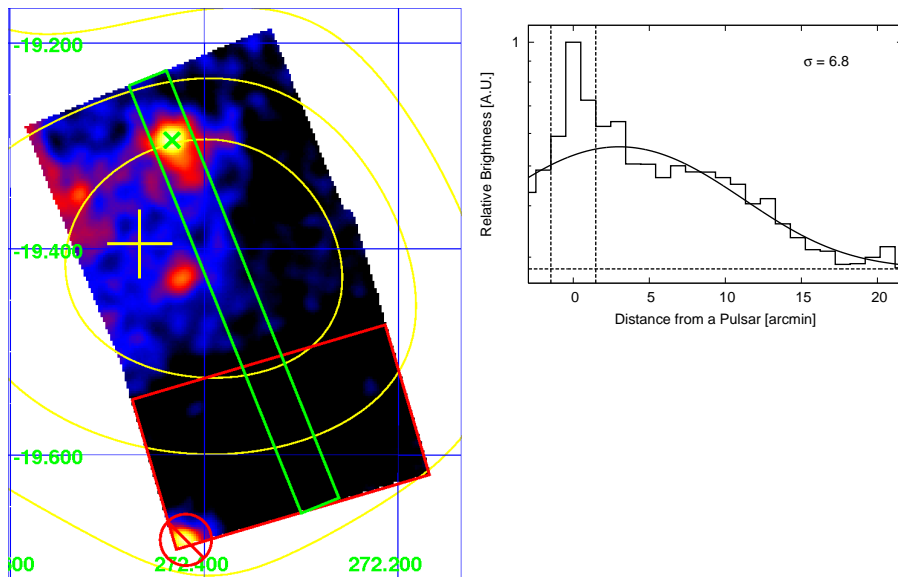


Fig. 2. Left: Suzaku XIS image of the region including HESS J1809–193. The pseudo-color represents vignetting-corrected, log-scaled intensity levels in the 2.0–10.0 keV band. The yellow cross indicates the centroid of HESS J1809–193, and the yellow lines represent 80%, 60%, and 40% contour of the peak of the VHE γ -ray (Renaud et al. 2008). Right: normalized 1-dimensional profile of the surface brightness in the 2.0–10.0 keV band along the direction from north to south in the green rectangle indicated in figure 2 with a spatial bin size of $1'.0$. Solid curve and horizontal dashed line show the best-fit Gaussian profile and a constant, respectively. The bright peak corresponding to the pulsar was ignored in this fit ($2'.9$ wide, inner part between the two vertical dashed lines).

3. Results

3.1. X-ray Image

In order to make images of this field, we corrected the vignetting effect by dividing the image by the flat sky image simulated using `xissim` (Ishisaki et al. 2007) after subtracting non X-ray background (Tawa et al. 2008). In this simulation, we assumed the input energy spectrum as that extracted from the red rectangular region (see §3.2). Hereafter, all images

are vignetting corrected. Figure 2 shows Suzaku XIS 2–10 keV image of the HESS J1809–193 region.

We confirmed largely extended emission reported by ASCA (Bamba et al. 2003a). In addition, we found the extended emission has several peaks. The pulsar is the brightest in the FOV, and the western edge of the FOV is also significantly bright, which was already hinted by ASCA (Bamba et al. 2003a).

We have determined extension of the diffuse emission as follows: We created a 1-dimensional profile of the surface brightness from the rectangle region shown in figure 2 (left) which runs from north to south. We selected the direction which enabled us to create the longest profile. We did not take a symmetric region around the pulsar, because the faint and diffuse emission is significantly asymmetric. Although there is a point source in the south of the pulsar at (272.42, -19.43), its flux in the integrated region is only 1 % of the central pulsar, thus negligible. The 1-dimensional profile thus created is shown in figure 2 (right). Note that the surface brightness is normalized to the peak brightness. We fitted the profile with a Gaussian function plus a constant to evaluate its extension. In the fitting, we ignored the brightest part around the pulsar with a width of $2'.9$ (corresponding to the point-spread function of the XRT). Consequently, we found the diffuse emission extends up to $\sim 20'$ away from the pulsar. The Gaussian center was found to be offset by $\sim 3'$ from the pulsar and the rms width to be $\sigma = 7' \pm 1'$.

3.2. Energy Spectra

We studied spatial variation of the X-ray energy spectra of the diffuse emission. We generated the detector response file and an auxiliary response file using `xisrmfgen`, and `xissimarfgen` (Ishisaki et al. 2007) and performed model fitting using XSPEC version 12.4.0.

First we examined energy spectrum from an outskirts of the HESS source region (the red rectangular region in figure 2) in order to estimate contribution of the Galactic Ridge X-ray Emission (GRXE) on this particular area. The bright source at the south-east corner (circled in red) was excluded in this analysis. We subtracted the non X-ray background (NXB) estimated using `xisnxbgen` (detail of the method described in Tawa et al. 2008), and averaged all of the available XISs (XIS 0,1,3) data. Because the NXB becomes high above 7.2 keV (in particular for XIS1 which has the back-illuminated chip), we used the data only below 7.2 keV. We fitted the spectra in 4.0–7.2 keV and 2.0–4.0 keV separately following the reproduction procedure of GRXE in Ebisawa et al. (2008). The model adopted is a power-law plus three narrow Gaussian (intrinsic width fixed to zero) in 4.0 – 7.2 keV, or four gaussian lines in 2.0 – 4.0 keV. The spectra and the best-fit models are shown in figure 3. The equivalent widths of the iron lines are summarized in table 2. These equivalent widths are comparable to those of GRXE described in Ebisawa et al. (2008). Thus we conclude that the X-ray emission in this region can be regarded as pure GRXE and no significant contribution from the pulsar is present.

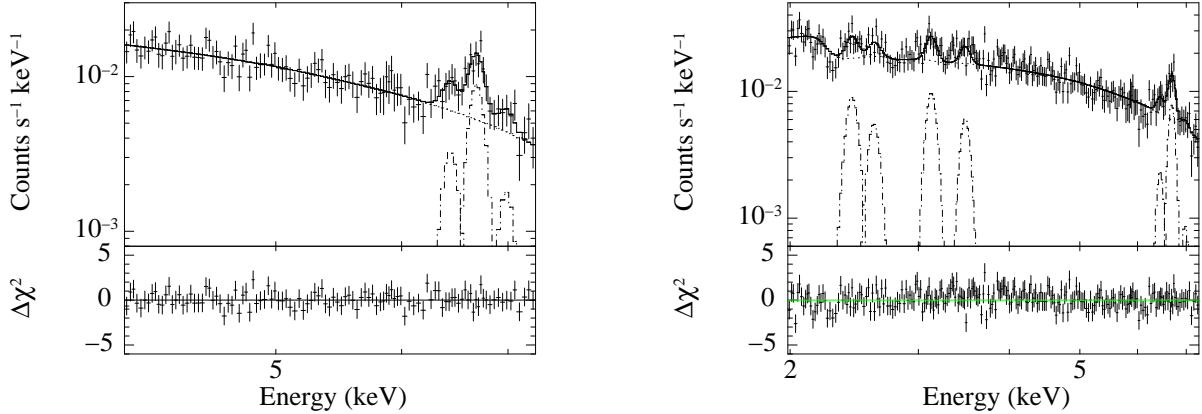


Fig. 3. Left: NXB-subtracted XIS spectrum in the 4.0–7.2 keV band extracted from the region enclosed with a red rectangle in figure 2 (left). The best-fit model, an absorbed power-law with three iron lines, is also shown in a solid line (each component in a dot-dashed line). The bottom panel shows residuals to the best-fit model. Right: the same as the left one, but in the 2.0–7.2 keV band. Narrow Gaussians were added to the model below 4 keV.

Table 2. Center energies and equivalent widths of the iron lines in the background region in comparison of those of the GRXE.

Background region			
Center energy (keV)	6.44 ± 0.07	6.69 ± 0.02	6.98 ± 0.08
Equivalent width (eV)	70 (0–140)	240 (160–550)	50 (0–170)
GRXE*			
Center Energy (keV)	6.41 ± 0.02	6.670 ± 0.006	7.00 ± 0.03
Equivalent width (eV)	80 (60–100)	350 (310–390)	70 (40–100)

Note. – Errors represent single-parameter 90% confidence limit.

* Center energies and equivalent widths determined by the GRXE observation with Suzaku by Ebisawa et al. (2008).

In the next step, we divided the sky region of the north pointing into a “check pattern” as shown in figure 4 (left) in order to find out the possible spatial variations of the spectral slope. Here we refer to these regions as the number indicated in figure 4 (left) with the prefix “Grid” (Grid1, Grid2, ...). We used a two component model for the fit: an absorbed power-law plus the GRXE. We used the model GRXE spectrum (as explained below) to subtract the diffuse background.

The model GRXE spectrum was constructed as follows: The background spectrum was fitted in the 2.0–7.2 keV band with the model of an absorbed power-law plus 7 narrow Gaussians as explained above. The absorption column density was fixed to $1.0 \times 10^{22} \text{ cm}^{-2}$. The best-fit parameters, besides the iron line parameters in table 2, are listed in table 3. Normalization for each extraction region was adjusted taking account of differences of the vignetting effects, size of the extraction region, and exposure time between the north and south pointings. The correction

Table 3. Best-fit parameters of an absorbed power-law model with emission lines.

Model component	Parameter	Value
Continuum	NH (10^{22} cm $^{-2}$)	1.0 (fixed)
	Γ	$1.40^{+0.05}_{-0.06}$
Emission lines	Energy (keV) S XV	2.43 ± 0.02
	S XVI	2.61 ± 0.04
	Ar XVII	3.13 ± 0.02
	Ar XVIII	$3.43^{+0.13}_{-0.07}$

Note. — Errors represent single-parameter 90% confidence limit.

factors of the vignetting effect (shown in figure 4 right) were determined by simulation. We subtracted the non X-ray background (NXB) estimated by using `xisnxbgen`. Figure 6 shows the XIS spectra (averaged for XIS 0, 1 and 3) and the best-fit models for all the 16 regions in the 2.0–10 keV band. Because Grid 1, 4, 13 were illuminated with the calibration sources, the data between 5.73–6.67 keV were removed from the fit. Fit results are summarized in table 4. The spatial distribution of the spectral indices is shown in figure 5. In order to make statistics better, we also fit the combined spectra of Grid 6 and 7 (for the region close to the emission peak) and Grid 11, 14, and 15 (for the region far from the emission peak). The results are included in Table 4. From these analyses, we concluded that there is no systematic trend of the spatial variations in the spectral index in this field of view.

4. Discussion

Using Suzaku, we have clearly shown presence of the large scale diffuse emission around HESS J1809–193, which was already suggested by ASCA (Bamba et al. 2003a). The extension of the diffuse emission is at least $\sim 21'$ (3σ of the gaussian approximation). The diffuse spectrum has the photon index of $\Gamma \sim 1.7$, which is much harder than those of SNRs with synchrotron X-ray emitting shells ($\Gamma \sim 2-3$), such as SN 1006, RX J1713–3946, and others (Bamba et al. 2008; Takahashi et al. 2008, for example). Such a hard spectrum, on the other hand, reminds us the PWN origin (Kargaltsev & Pavlov 2008). This hypothesis is, in fact, strengthened by the very existence of the pulsar PSR J1809–1917.

The TeV emission also may have the PWN origin, because it positionally coincides with the region including the pulsar and the diffuse X-ray emission, although the center of the TeV emission is offset by $\sim 6'$ (a projected distance of 6 pc at 3.5 kpc) from the pulsar. If both the TeV and X-ray emissions are from the same PWN, their origin is accelerated electrons via inverse Compton (TeV) and synchrotron mechanisms (X-ray). Typical energies of responsible electrons are ~ 20 TeV for the TeV emission and ~ 80 TeV for X-rays, respectively. The former has much longer synchrotron life timescales than latter (Mattana et al. 2009, for example). If

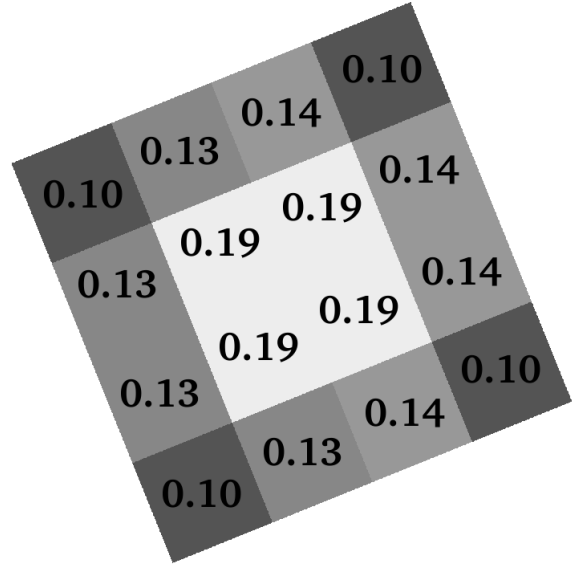
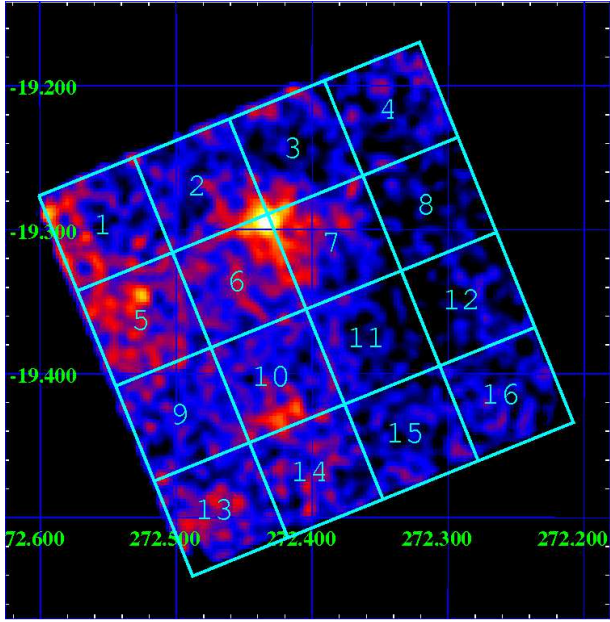


Fig. 4. Left: Suzaku XIS image of the north pointing in the 2.0-10.0 keV band and designation of the 16 sub-regions for spectral variation study. Right: Correction factors for each region, which take account of the vignetting effects, differences of the exposure and the extraction area between the source region and the GRXE region (the red rectangle in figure 2).

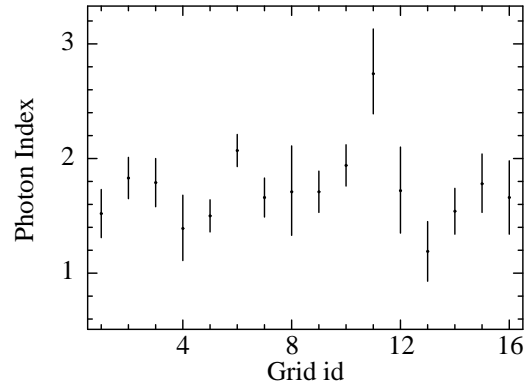
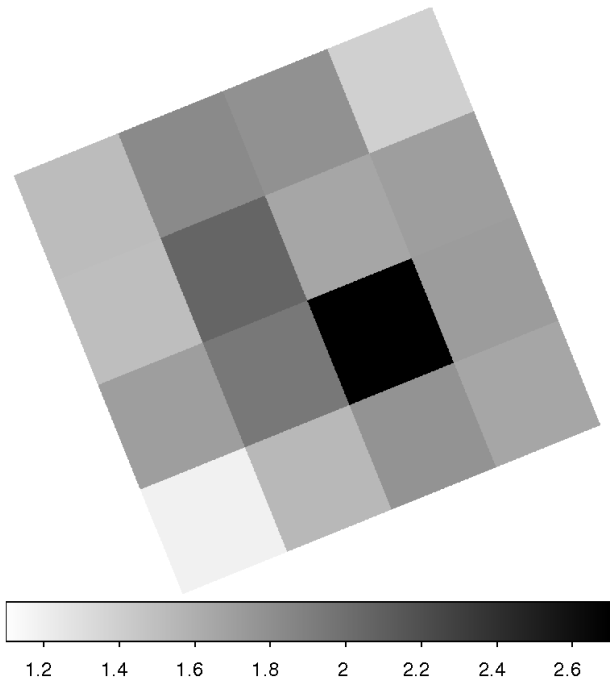


Fig. 5. Spatial distribution of the spectral indices around PSR J1809-1917. Left: best-fit photon index map. Gray scale indicates the photon indices; light gray means the spectrum is hard while dark gray means soft. Right: photon indices of each grid with 90% error bars.

Table 4. Best-fit parameters of an absorbed power-law model for each grid.

Grid id	Γ	Flux* (10^{-13} ergs cm $^{-2}$ s $^{-1}$)	χ^2 /d.o.f.
1	1.52 ± 0.21	8.7 ± 0.9	52.2/46
2	1.83 ± 0.18	7.8 ± 0.6	70.6/67
3	1.79 ± 0.21	5.9 ± 0.6	54.1/62
4	1.39 ± 0.28	$6.1^{+0.9}_{-0.8}$	49.1/37
5	1.50 ± 0.14	10.6 ± 0.7	74.0/73
6 [†]	2.07 ± 0.14	8.2 ± 0.5	105.0/102
7 [†]	1.66 ± 0.17	6.7 ± 0.5	121.7/93
8	$1.71^{+0.40}_{-0.38}$	3.0 ± 0.5	59.2/48
9	1.71 ± 0.18	7.1 ± 0.6	58.1/61
10	1.94 ± 0.18	5.9 ± 0.5	122.9/86
11	$2.74^{+0.39}_{-0.35}$	2.4 ± 0.4	87.6/70
12	$1.72^{+0.38}_{-0.37}$	2.9 ± 0.5	65.2/47
13	1.19 ± 0.26	8.3 ± 1.0	51.4/41
14	1.54 ± 0.20	$7.2^{+0.7}_{-0.6}$	74.3/59
15	1.78 ± 0.25	$4.4^{+0.6}_{-0.5}$	55.5/52
16	1.66 ± 0.32	4.9 ± 0.7	60.8/40
6 [†] +7 [†]	1.91 ± 0.11	14.7 ± 0.9	235.9/196
11+14+15	1.84 ± 0.14	$13.7^{+1.5}_{-1.4}$	243.2/183

Note. — Errors represent single-parameter 90% confidence limit.

* Unabsorbed flux in the 2.0–10.0 keV band.

† The emission is dominated by the point source.

we assume that the electrons which emit TeV gamma-rays have the same age as the pulsar ($\tau c = 51$ kyr) and those for the X-rays are very fresh, the positional offset may be explained by the proper motion of the pulsar. To explain the offset of $\sim 6'$, the transverse velocity of the pulsar needs to be ~ 120 km s $^{-1}$, which can be explained with the average transverse velocity of radio pulsars (Lyne & Lorimer 1994, ~ 300 km s $^{-1}$). **On the other hand, the tails seen in the *Chandra* image (if it is indeed a tail not a jet) suggests that the pulsar is moving southward and its velocity vector is at the angle of ~ 190 – 200 deg. East of North (Kargaltsev & Pavlov 2007). Now if we assume that the pulsar was born at the center of the TeV source and moved to its current position, its velocity vector would have to be at the angle of 10 – 20 deg. West of North. Therefore, the angle between these two velocity vectors will be ~ 140 – 160 deg., which makes this scenario unlikely.** Another possible scenario to make such an offset is collision between the reverse shock and the PWN (Pavlov et al. 2008) like the case for Vela X (Blondin et al. 2001; Gaensler et al. 2003).

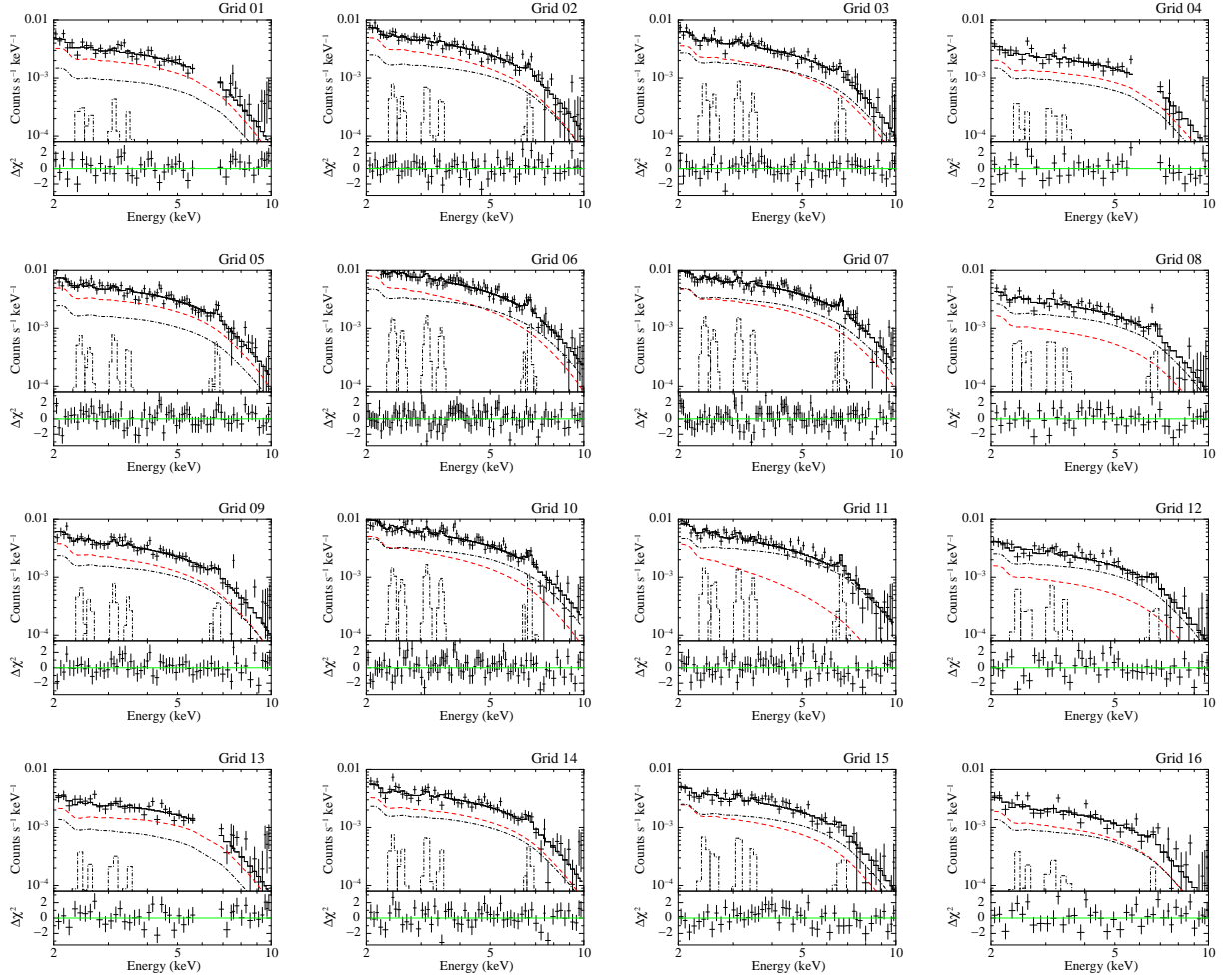


Fig. 6. NXB-subtracted XIS spectra in the 2.0–10.0 keV band extracted from each grid shown in figure 4. Dashed line, dash-dot line and dash-dot histograms indicate the best-fit absorbed power-law model, a GRXE model and emission lines, respectively.

In the young PWNe, it is suggested that the X-ray spectra become softer with the distance from the pulsars due to synchrotron energy loss of the accelerated electrons (Mori et al. 2004, for example). However, we could not find any hint of such softening (Figure 5). This means that electrons do not lose significant energies via the synchrotron emission. The X-ray size of HESS J1809–193 is $\sim 21'$ ($= 3\sigma$), or 21 pc with the assumed distance of 3.5 kpc. The synchrotron lifetime of an accelerated electrons (τ_{syn}) is $\tau_{syn} = 6.8 \text{kyr} (B/3 \mu\text{G})^{-3/2} (E_{syn}/2 \text{keV})^{-1/2}$, where B and E_{syn} are magnetic field and mean energy of synchrotron emission from accelerated electrons, respectively. In order to explain the size of the X-ray diffuse emission, the transport velocity of accelerated electrons should be higher than $21 \text{pc}/\tau_{syn} \sim 3.0 \times 10^3 \text{km s}^{-1} (B/3 \mu\text{G})^{3/2} (E_{syn}/2 \text{keV})^{1/2}$, which seems to be very fast for an old PWN, and even comparable to the forward shock velocities of young SNRs. It is known that the diffusion coefficient in young PWNe and SNRs is too small to diffuse out

to such a large scale, when the magnetic field is turbulent (Shibata et al. 2003; Bamba et al. 2003b; Bamba et al. 2005, for example). Therefore, the current observation suggests that the turbulence of magnetic fields in old PWN systems are smaller than those in young systems. If turbulence of the magnetic fields in old PWN systems is smaller than that in young systems, such a fast diffusion may be explained, although we have no such a model for old PWNe. In supernova remnants, we have some indication that the turbulence becomes smaller when the SNR becomes older (Bamba et al. 2005), similar mechanism might work for PWNe.

We have a similar case, HESS J1825–137, which is another unID TeV source with possible PWN origin. Uchiyama et al. (2009) found that the X-ray photon index is nearly constant over the emission region, which may suggest HESS J1825–137 also might have small turbulence of the magnetic field. Therefore, we suppose fast transportations of accelerated electrons may be rather common phenomena in old PWNe. Further similar samples of unID TeV sources may confirm this hypothesis.

5. Summary

- We observed the TeV PWN candidate HESS J1809–193 with Suzaku, and confirmed an extended emission around the pulsar PSR J1809–1917. Size of the X-ray emission is at least $\sim 21'$, or 21 pc at 3.5 kpc.
- The extended emission has very hard nonthermal spectrum with the photon index of ~ 1.7 . No systematic spatial variation of the photon index is found, which implies that accelerated electrons do not lose their energy when they run from the pulsar to the edge of the emission region. We have to consider very fast diffusion in an old PWN to reproduce such phenomena. If turbulence of the magnetic fields in old PWN systems is smaller than that in young systems, such a fast diffusion may be explained.

Acknowledgements

We would like to thank the anonymous referee for useful comments and suggestions. We acknowledge all the Suzaku team members for their gracious supports. The authors also thank K. Mori and R. Yamazaki for their fruitful comments. A. Bamba is supported by JSPS Research Fellowship for Young Scientists (19-1804).

References

- Aharonian, F., et al. 2005a, *Science*, 307, 1938
Aharonian, F., et al. 2006a, *ApJ*, 636, 777
Aharonian, F., et al. 2006b, *A&A*, 460, 365
Aharonian, F., et al. 2007, *A&A*, 472, 489
Aharonian, F., et al. 2008, *A&A*, 477, 353

Anada, T., Ebisawa, K., Dotani, T., & Bamba, A. 2009, PASJ, 61, 183

Bamba, A., Ueno, M., Koyama, K., & Yamauchi, S. 2003a, ApJ, 589, 253

Bamba, A., Yamazaki, R., Ueno, M., & Koyama, K. 2003b, ApJ, 589, 827

Bamba, A., Yamazaki, R., Yoshida, T., Terasawa, T., & Koyama, K. 2005, ApJ, 621, 793

Bamba, A., et al. 2008, PASJ, 60, 153

Blondin, J. M., Chevalier, R. A., & Frierson, D. M. 2001, ApJ, 563, 806

Cordes, J. M., & Lazio, T. J. W. 2002, arXiv:astro-ph/0207156

Ebisawa, K., et al. 2008, PASJ, 60, 223

Gaensler, B. M., Schulz, N. S., Kaspi, V. M., Pivovarov, M. J., & Becker, W. E. 2003, ApJ, 588, 441

Hinton, J. 2007, ArXiv e-prints, 712, arXiv:0712.3352

Ioka, K., & Meszaros, P. 2009, arXiv:0901.0744

Ishisaki, Y., et al. 2007, PASJ, 59, 113

Kargaltsev, O., & Pavlov, G. G. 2007, ApJ, 670, 655

Kargaltsev, O., & Pavlov, G. G. 2008, 40 Years of Pulsars: Millisecond Pulsars, Magnetars and More, 983, 171 (Astro-ph/0801.2602)

Kokubun, M., et al. 2007, PASJ, 59, 53

Komin, N., Carrigan, S., Djannati-Ataï, A., Gallant, Y. A., Kosack, K., Puehlhofer, G., Schwemmer, S., & for the H. E. S. S. Collaboration 2007, arXiv:0709.2432

Koyama, K., et al. 2007, PASJ, 59, 23

Lyne, A. G., & Lorimer, D. R. 1994, Nature, 369, 127

Mattana, F., et al. 2009, ApJ, 694, 12

Mewe, R., Gronenschild, E. H. B. M., & van den Oord, G. H. J. 1985, A&AS, 62, 197

Mitsuda, K. et al. 2007, PASJ, 59, S1

Mori, K., Burrows, D. N., Hester, J. J., Pavlov, G. G., Shibata, S., & Tsunemi, H. 2004, ApJ, 609, 186

Morris, D. J., et al. 2002, MNRAS, 335, 275

Nakajima, H., et al. 2008, PASJ, 60, 1

Nakamura, R., Bamba, A., Ishida, M., Nakajima, H., Yamazaki, R., Terada, Y., Pühlhofer, G., & Wagner, S. J. 2009, PASJ, 61, 197

Pavlov, G. G., Kargaltsev, O., & Briskin, W. F. 2008, ApJ, 675, 683

Renaud, M., Hoppe, S., Komin, N., Moulin, E., Marandon, V., & Clapson, A.-C. 2008, American Institute of Physics Conference Series, 1085, 285

Serlemitsos, P. J., et al. 2007, PASJ, 59, 9

Shibata, S., Tomatsuri, H., Shimanuki, M., Saito, K., & Mori, K. 2003, MNRAS, 346, 841

Takahashi, T., et al. 2007, PASJ, 59, 35

Takahashi, T., et al. 2008, PASJ, 60, 131

Tawa, N., et al. 2008, PASJ, 60, 11

Uchiyama, H., Matsumoto, H., Tsuru, T. G., Koyama, K., & Bamba, A. 2009, PASJ, 61, S189

Yamazaki, R., Kohri, K., Bamba, A., Yoshida, T., Tsuribe, T., & Takahara, F. 2006, MNRAS, 371, 1975